



# Online dynamical downscaling of temperature and precipitation within the *i*LOVECLIM model (version 1.1)

Aurélien Quiquet<sup>1</sup>, Didier M. Roche<sup>1,2</sup>, Christophe Dumas<sup>1</sup>, and Didier Paillard<sup>1</sup>

<sup>1</sup>Laboratoire des Sciences du Climat et de l'Environnement, LSCE/IPSL, CEA-CNRS-UVSQ, Université Paris-Saclay, F-91191 Gif-sur-Yvette, France

<sup>2</sup>Earth and Climate Cluster, Faculty of Earth and Life Sciences, Vrije Universiteit Amsterdam, Amsterdam, the Netherlands

Correspondence to: A. Quiquet ([aurelien.quiquet@lsce.ipsl.fr](mailto:aurelien.quiquet@lsce.ipsl.fr))

## Abstract.

In this paper, we present the inclusion of an online dynamical downscaling of heat and moisture within the model of intermediate complexity *i*LOVECLIM v1.1. We describe the followed methodology to generate temperature and precipitation fields on a 40 km x 40 km Cartesian grid of the Northern Hemisphere from the T21 native atmospheric model grid. Our scheme is non grid-specific and conserves energy and moisture. We show that we are able to generate a high resolution field which presents a spatial variability in better agreement with the observations compared to the standard model. Whilst the large-scale model biases are not corrected, for selected model parameters, the downscaling can induce a better overall performance compared to the standard version on both the high-resolution grid and on the native grid. Foreseen applications of this new model feature includes ice sheet model coupling and high-resolution land surface model.

## 10 1 Introduction

In recent decades, the Earth is undergoing a sustained global warming due to a rapid rise of greenhouse gases, unprecedented over the last million years (Luthi et al., 2008; Wolff, 2011). Some components of the Earth system, such as the oceanic and terrestrial carbon cycles or the continental ice sheets, present feedbacks acting over long timescales, i.e. pluri-millennial, and are suspected to play an important role for the climate in the future (Archer and Brovkin, 2008). Earth models of intermediate complexity (EMICs) are powerful tools to investigate the long-term transient response of the climate system (Claussen et al., 2002). The advantage of these models is to include most of the major climatic components in a unified and coupled framework. They are also computationally unexpensive compared to more comprehensive general circulation models (GCMs) because of a simplified physics and a coarser resolution. As such, they can be used to perform numerous simulations to assess model sensitivities (e.g. Loutre et al., 2011) or multi-millenia integrations to study slow feedbacks (e.g. Calov et al., 2005).

20 However, the relative simplicity and coarse resolution of such climate models result in an approximative representation of land surface climatic variables that are affected by variability at high spatial resolution. Precipitation is an example of such a variable, being a key component of the climate system and nonetheless generally poorly represented in atmospheric models. In particular, EMICs are unable by design to reproduce correctly meso-scale atmospheric processes induced by sub-grid topography. This have important consequences for the sub-components of the climate system that depend on the atmospheric



water cycle such as surface hydrology and vegetation or water isotopes. High resolution is a particularly dire requirement for components whose physical description require a high spatial gridding. It has been a recurrent issue in climate-hydrology studies at basin scale (e.g. Vetter et al., 2015) as well as in ice sheet - climate coupling studies (e.g. Charbit et al., 2005; Fyke et al., 2011).

5 Ice sheet models in particular need a high resolution to represent grounding line dynamics (Schoof, 2007) and to account for narrow ablation zones at the margins (Ettema et al., 2009). To account for it, ice sheet – climate coupled models have often preferred to use their own anomalies regridded on top of a reference climate to force the ice sheet model (e.g. Vizcaíno et al., 2008; Goelzer et al., 2016). The anomalies are then linearly interpolated and superimposed to well-constrained and high-resolution present-day climate fields. Such a strategy implicitly assumes that the model biases remain unchanged through time, inde-  
10 pendently from the imposed external forcings. Alternatively, an other strategy is to use absolute fields, but downscaled to the needed resolution. The complexity of such downscaling approaches ranges from simple bi-linear interpolations (e.g. Vizcaíno et al., 2010; Gregory et al., 2012) to more physically based approaches. To achieve temperature downscaling, Charbit et al. (2005) duplicate the energy budget calculation on 15 artificial levels in order to retrieve surface temperature on a vertically  
15 artificial levels. Alternatively, Robinson et al. (2010) embed a simplified regional energy-moisture balance model in order to assess sub-grid processes unresolved by their native atmospheric model. Although statistical downscaling has been applied to EMIC outputs (Vrac et al., 2007; Levavasseur et al., 2011), these techniques were not used to couple different components of models.

20 Here, we present the inclusion of a relatively unexpensive online and conservative dynamical downscaling of heat and moisture in the *iLOVECLIM* coupled climate model (version 1.1). The downscaling is done from the native T21 grid ( $\simeq 5.625^\circ$  spatial resolution) towards a cartesian 40 km x 40 km grid of the Northern Hemisphere. The chosen high resolution grid arises from the ice sheet model grid embedded in *iLOVECLIM* (Roche et al., 2014). Computed on each atmospheric timestep, the downscaling accounts for the feedback of sub-grid precipitation on large scale energy and water budget, thus being energy and moisture  
25 conservative. This property, i.e. a closed water budget, is particularly important for multi-millenia simulations. The downscaling methodology is not grid-specific and could be applied in the future to any grid having a higher resolution than the native T21 grid. In particular, downscaling over only a certain region (e.g. Europe or the Andes) is possible with our implementation. Foreseen applications include ice-sheet surface mass balance computation and land surface modelling (hydrology, permafrost, land carbon) at continental scale and high resolution.

30

In Sec. 2 we describe the implementation of the dynamical downscaling of heat and moisture in the atmospheric component of the *iLOVECLIM* model. In Sec. 3 we discuss the performance of both the standard and downscaled temperature and precipitation fields in representing present-day climatological fields. We list concluding remarks and perspectives in Sec. 4.



## 2 Methodology

### 2.1 the *i*LOVECLIM model

*i*LOVECLIM (here in version 1.1) is a code fork of the LOVECLIM 1.2 model, extensively described in Goosse et al. (2010). Whilst the physics in the atmosphere, ocean and land surface has remained mostly unchanged, the major bifurcations from Goosse et al. (2010) consist in the addition of a water oxygen isotope cycle (Roche, 2013; Roche and Caley, 2013), an oceanic carbon model (Bouttes et al., 2015), an alternative ice sheet model (Roche et al., 2014), the reimplementation of the initial iceberg model (Bügelmayer et al., 2015), and a permafrost model (Kitover et al., 2015). The atmospheric component of main concern here, ECBilt, is a quasi-geostrophic model, solved on a T21 spectral grid. For a complete description of ECBilt, the reader is referred to Haarsma et al. (1997) and Opsteegh et al. (1998) and references therein. The dynamics, i.e. the resolution of the potential vorticity equation, is computed for three vertical levels: 800 hPa, 500 hPa and 200 hPa. The equations for temperature and vertical motion are computed on two intermediate levels at 650 hPa and 350 hPa.

The main idea of the downscaling procedure is to replicate the processes governing precipitation formation and surface temperature computation on a refined vertical extended grid in order to assess these variables at any altitude for any given sub-grid.

### 2.2 Vertical profiles of heat and moisture

The first steps of the downscaling is to recompute heat and moisture variables on a vertically extended grid of the atmosphere. In the following, we present the equations already described in Haarsma et al. (1997), which are needed for the vertically extended grid.

#### 2.2.1 Temperature profile

In ECBilt, due to the lack of a proper representation of the atmospheric boundary layer, an idealised vertical profile is used to compute heat, moisture and momentum fluxes at the Earth surface. Above 200 hPa, the atmosphere is assumed to be isothermal. From the 650 hPa and 350 Pa intermediate levels, we compute a linear temperature profile in the logarithm of pressure from 200 hPa to the surface.

Thus, for any pressure level  $p$ , the temperature is:

$$T(p) = T_{650} + \gamma \ln \left( \frac{p}{p_{650}} \right) \quad (1)$$

With  $\gamma$  the atmospheric temperature lapse rate as:

$$\gamma = \frac{T_{350} - T_{650}}{\ln(p_{350}/p_{650})} \quad (2)$$



As in Haarsma et al. (1997), the near-surface air temperature is computed from  $T_{500}$  using Eq. 2 and assuming hydrostatic equilibrium and ideal gas law:

$$\bar{T}_* = \sqrt{T_{500}^2 - \frac{2\gamma g}{R} (\bar{z}_h - z_{500})} \quad (3)$$

With  $\bar{z}_h$  is the model surface height and  $z_{500}$  the height of the 500 hPa levels (prescribed homogeneously at 5500 m).

- 5 For the implementation of the downscaling, we define 11 artificial surfaces at fixed vertical height  $z_h (l = 1, 11)$ , on which the near-surface air temperature is calculated as:

$$T_*(l = 1, 11) = \sqrt{T_{500}^2 - \frac{2\gamma g}{R} (f_s z_h(l) - z_{500})} \quad (4)$$

The vertical lapse rate in temperature computed in the model in Eq. 2 is representative of the free-atmosphere temperature variations. Due to orography, the atmospheric isotherms are shifted upwards. As such, the temperature retrieved at the surface using the free-atmosphere lapse rate over-estimate the temperature changes with elevation. To account for this known effect, we apply a global tunable correcting factor,  $f_s$  in Eq. 4 (typically ranging from 0.5 to 1.), to the orography on the vertically extended grid.

From this near-surface air temperature for the artificial surfaces, we derive the different surface energy balance terms as described in Haarsma et al. (1997). Surface temperatures at the artificial surfaces  $T_s (l = 1, 11)$  are computed iteratively from the energy balance, assuming a zero heat capacity of the surface. We assume no change in surface types, and consequently albedo, between the different artificial layers. Because the latent heat flux depends on the evaporation, we also need to assess the specific humidity at the 11 artificial surface levels.

### 2.2.2 Moisture profile

In ECBilt, only the lower part of the atmosphere (i.e. below 500 hPa) contains water. A single equation is used to compute the evolution of total precipitable water  $\bar{q}_a$  from advection, precipitation and evaporation. In our version of the model, precipitation occurs when the total amount of precipitable water is greater than a fraction ( $\alpha_q = 90\%$ ) of the vertically integrated saturation specific humidity  $q_{max}$ . For each artificial level, the expression of  $q_{max} (l = 1, 11)$  is computed as in Haarsma et al. (1997):

$$q_{max}(l = 1, 11) = \frac{1}{\rho_w} \int_{p_0(l)}^{500hPa} q_s(T, p) \frac{dp}{g} \quad (5)$$

Where  $\rho_w$  is the water density,  $g$  is the gravitational acceleration and  $p_0 (l = 1, 11)$  the surface pressure computed with Eq. 2:

$$25 \quad p_0(l = 1, 11) = p_{650} \exp\left(\frac{T_*(l) - T_{650}}{\gamma}\right) \quad (6)$$

The saturation specific humidity at a given level,  $q_s(T, p)$ , is given by a Clausius-Clapeyron expression of the saturation vapour pressure. The vertical profile of specific humidity is retrieved assuming a constant relative humidity for the whole atmospheric column below 500 hPa.



## 2.3 Sub-grid precipitation and coarse grid upscaling

### 2.3.1 From the vertically extended grid to the sub-grid

For a given native coarse-grid point at a given surface height  $\bar{z}_h$ , we have a certain numbers of sub-grid points  $k$  of different surface heights  $z_h(k=1, k_{max})$ . The surface elevation in the native grid can be computed as:

$$5 \quad \bar{z}_h = \frac{1}{k_{max}} \frac{\sum_{k=1}^{k_{max}} (z_h(k) s_a(k))}{\sum_{k=1}^{k_{max}} s_a(k)} \quad (7)$$

Where  $s_a(k)$  is the surface of the sub-grid cell.

In order to compute the heat and moisture budget on a sub-grid point  $k$ , we linearly interpolate a needed surface variable  $\phi$  from the two neighbouring vertical artificial levels  $l$  and  $l+1$ :

$$10 \quad \phi(k=1, k_{max}) = \frac{z_h(l) - z_h(k)}{z_h(l) - z_h(l+1)} \phi(l) + \left(1 - \frac{z_h(l) - z_h(k)}{z_h(l) - z_h(l+1)}\right) \phi(l+1) \quad (8)$$

Thus, from the variables computed on the vertically extended grid, we recompute on the sub-grid: the near-surface air temperature  $T_*$ , the surface temperature  $T_s$  and integrated saturation specific humidity  $q_{max}$ .

15 Winds are not downscaled in our approach. In the real world, orographic precipitation mostly occurs on wind-faced slopes whilst the other side is generally much drier. On the native grid of ECBilt, winds transport humidity and thus affect precipitation amounts. For our downscaling approach, because winds are not downscaled, in order to mimic the enhancement of precipitation on wind-faced slopes, we could sort the sub-grid points depending on winds. We discard this approach computationally expensive. Instead, we sort the sub-grid points by elevation for a given coarse grid point so that the lowlands before the mountain ranges are treated before the higher altitudes. The lowest grid point is initialised to the coarse-grid value:  $q_a(k=1) = q_a$ . As we compute precipitation for a sorted sub-grid point, we remove available precipitable water from the amount of total precipitable water of the previous grid point. In doing so, we assume that the mountain edges (lowest elevations) are the first affected by moisture influx.

### 2.3.2 Dynamic precipitation

25 Two processes are responsible for dynamic precipitation in ECBilt. First, since the upper atmospheric layer (above 500 hPa) is assumed to be dry, any vertical moisture export through the 500 hPa level is converted into precipitation. The amount of this export is calculated from the moisture availability at 500 hPa, which depends of the local surface topography. For this reason, we expand the computation of moisture export on the vertically expended grid. Following a similar expression as in Haarsma et al. (1997), in case of a negative vertical velocity at 500 hPa,  $\omega$ , the amount of precipitation on an atmospheric timestep (4 hours) is:

$$30 \quad p_{dyn,ve}(l=1, 11) = -\omega q_*(l) / \rho_w g \quad (9)$$



where  $q_*$  the precipitable water given by:

$$q_*(l = 1, 11) = r(l) q_s(p = 500 \text{ hPa}) \quad (10)$$

with  $r$  the relative humidity, which depends on the local topography since its computation is derived from the vertically integrated saturated specific humidity (Eq. 5):

$$r(l = 1, 11) = q_a / q_{max}(l) \quad (11)$$

From the dynamic precipitation on the vertically extended grid,  $p_{dyn,ve}(l = 1, 11)$ , we compute the corresponding sub-grid precipitation,  $p_{dyn,ve}(k = 1, k_{max})$ , with Eq.8 linear interpolation.

An other contribution to dynamic precipitation is due to moisture excess. In the version of ECBilt included in iLOVECLIM v1.1, dynamic precipitation occurs when the total amount of precipitable water, is greater than  $\alpha_q = 90\%$  of the vertically integrated saturation specific humidity. On the sub-grid points a similar condition is checked, based on the local total amount of precipitable water,  $q_a(k = 1, k_{max})$ , and the local vertically integrated saturation specific humidity  $q_{max}(k = 1, k_{max})$ . In the original version of ECBilt, the value for  $\alpha_q$  has been tuned to reproduce the global scale precipitation pattern. Because of the higher spatial variability in topography, the downscaling induces a change in the precipitation pattern. There is no reason why this tuned  $\alpha_q$  should be kept unchanged from the original model. In addition, because of the strong non-linearity of the precipitation to elevation, we add the possibility to modify the value of  $\alpha_q$  depending on the local elevation  $z_h(l = 1, k_{max})$ :

$$\alpha_q(k = 1, k_{max}) = \min\left(\alpha_q^{min} + (1 - \alpha_q^{min}) \frac{z_h(k)}{z_q}, 1\right) \quad (12)$$

where  $\alpha_q^{min}$  is the value for a point at sea level and  $z_q$  is the altitude above which the precipitation occurs only if the total precipitable water reaches 100% saturation. As in Haarsma et al. (1997), dynamic precipitation due to moisture excess is expressed as:

$$p_{dyn,mc}(k = 1, k_{max}) = \frac{q_a - \alpha_q(k) q_{max}(k)}{C_{lh}(k) * dt} \quad (13)$$

With  $dt$  the atmospheric model timestep (4 hours) and  $C_{lh}$  a corrective term to account for latent heat release in the atmosphere associated with the precipitation:

$$C_{lh}(k = 1, k_{max}) = 1. + \frac{r(k) \rho_w L_c g}{c_p \Delta p_l} \left( \frac{dq_{max}}{dT_{650}} \right) (k) \quad (14)$$

With  $L_c$  the latent heat of condensation,  $c_p$  the specific heat capacity and  $\Delta p_l$  the lower layer depth (500 hPa).  $\frac{dq_{max}}{dT_{350}}$  is obtained from tabulated values of Eq. 5.

For the two contributions of dynamic precipitation, the near-surface air temperature of the sub-grid,  $T_*(k = 1, k_{max})$ , is used to determine snow and rain partition with an abrupt transition at 0 °C. Similarly to what is done for coarse grid precipitation in the standard version of ECBilt (Haarsma et al., 1997; Opsteegh et al., 1998), the sub-grid dynamic precipitations, either snow and rain, are associated with a local release of heat at 350 hPa, modifying  $T_{350}(k = 1, k_{max})$ .



### 2.3.3 Convective precipitation

Convective precipitation is assumed to be an adjustment term to reach stability in the atmospheric column. After a first dynamic precipitation removal, we compute convective precipitation only if  $q_a(k=1, k_{max})$  is still greater than  $\alpha_q(k) q_{max}(k)$ . The amount of convective precipitation,  $p_{conv}(k=1, k_{max})$ , is computed with the same formulation as in Eq. 13. We assess stability comparing the moist adiabatic lapse rate to the local potential temperature at 500 hPa,  $\theta(k=1, k_{max})$ , computed from the potential temperatures at 350 hPa and 650 hPa. Because sub-grid precipitation affects the local vertical lapse rate due to latent heat release, we need to compute the convective columns for each individual sub-grid points. This is an iterative process and we only go to the next sub-grid point when we reach stability locally.

### 2.3.4 Upscaling to the coarse grid

Following the dynamic and convective iterations on the sub-grid, moisture and energy on the native grid have to be updated. On the one hand, the initial coarse-grid moisture is simply reduced by the sum of sub-grid total precipitations, hence readily conserving water. On the other hand, the temperatures at 350 hPa and 650 hPa are recomputed as the mean of the sub-grid temperatures at these levels.

## 3 Application and validation

### 3.1 Sub-grid of the Northern Hemisphere

As an example application, we use a sub-grid domain covering a large part of the Northern Hemisphere (hereafter NH40, Fig. 1). The sub-grid topography comes from ETOPO1 (Amante and Eakins, 2009), projected with a Lambert equal-area projection onto a squared 40 km x 40 km Cartesian grid. The grid contains 241x241 points with more than half of the domain being continental areas. This grid was chosen because it corresponds to the ice sheet model grid embedded in *iLOVECLIM*. The T21 topography depicted in Fig. 1 corresponds to the NH40 topography aggregated to the native model resolution. This is the topography seen by the model when the downscaling is not performed.

#### 3.1.1 Experimental design

For model evaluation, we define a control simulation (hereafter CTRL) as a 100 years of *iLOVECLIM* integration under constant pre-industrial external forcing. With the same experimental design, we define a series of downscaling experiments in which we compute the heat and moisture budgets on the NH40 grid. For these experiments, we test the importance of three selected parameters: the elevation from which 100% saturation is needed to initiate precipitation  $z_q$  in Eq. 12 (2000 and 3500 m), the minimum fraction of saturation to initiate precipitation  $\alpha_q^{min}$  in Eq. 12 (0.7, 0.75, 0.8, 0.85, 0.9) and the mountain scaling factor  $f_s$  in Eq. 4 (0.6, 0.7, 0.8, 0.9 and 1.). We explore the whole matrix of runs, which corresponds to 50 model realisations. For notations purposes, the downscaling experiments are noted  $DOWN_{ijk}$ , with:



- $i = 0, 1$  for  $z_q = 2000m$  or  $z_q = 3500m$ ;
- $j = 0, 1, 2, 3, 4$  for  $\alpha_q^{min}$  from 0.7 to 0.9, by 0.5;
- $k = 0, 1, 2, 3, 4$  for  $f_s$  from 0.6 to 1.0, by 1.0.

For example, DOWN<sub>023</sub> uses  $z_q = 2000m$ ,  $\alpha_q^{min} = 0.8$ ,  $f_s = 0.9$ . The downscaling increases the computation time by roughly  
5 40%.

### 3.2 Model evaluation

For model evaluation, we compare the modelled annual mean climatic fields, namely surface temperature and precipitation rate, to observation-derived dataset. For this, we use a 1970-1999 climatological mean of annual surface temperature of ERA-interim reanalysis (Dee et al., 2011) and the long-term mean climatology of annual precipitation of CRU CL-v2 (New et al.,  
10 2002). We use ERA-interim on the  $0.125^\circ \times 0.125^\circ$  resolution for the whole Northern Hemisphere, whilst CRU CL-v2 covers the whole continental areas on a 10 min grid. We use bilinear interpolation to generate this data on the NH40 grid. For diagnostic purposes we also aggregate this data on the T21 grid with the same grid correspondance already used in Roche et al. (2014).

#### 3.2.1 Surface temperature

The annual mean surface temperature for ERA-interim and model outputs on the NH40 and T21 grids is presented in Fig. 2.  
15 On the one hand, the general pattern, i.e. the strong latitudinal cooling, is generally well represented in the CTRL experiment. If the strong continentality over Siberia is captured, the model is generally largely too warm, in particular over North America, Greenland and Western Europe. The temperature anomaly induced by local topography in the CTRL experiment is also largely underestimated. On the other hand, at the continental scale, our downscaling procedure does not imply important changes in surface temperature. This suggests that the downscaling has only a minor impact on atmospheric circulation. However, the  
20 downscaling induces important local temperature changes, particularly visible on the NH40 grid.

In Fig. 3, we present the annual mean surface temperature for a selection of downscaling experiments across selected transects: West to East for Europe and North America and South to North for Greenland (dashed purple lines in Fig. 2). ERA-interim temperature shows a strong dependency to elevation. This dependency is remarkably well reproduced for the European  
25 transect. However, the warm model bias is only reduced for elevated areas, with only a very limited change at lower elevation. This is because our downscaling methodology strongly relies on topography and is thus not designed to correct the model bias in lowland areas. For the other transects, even if the horizontal gradients are generally better reproduced with the downscaling, the large model bias in the original model induces large errors, only slightly corrected by the downscaling.

30 To assess general model performance, we present in Fig. 4 a normalised Taylor diagram computed from ERA-interim and several model outputs. In this figure, we present one selected downscaling experiment (namely DOWN<sub>020</sub>), as the sensitivity



of the Taylor diagram to model parameters is very limited. Overall, the model generally shows very good skills in reproducing annual mean surface temperatures, for both the CTRL and DOWN experiments (filled circles). In particular, the model presents a good spatial correlation (greater than 0.9) with a standard deviation generally slightly overestimated. Because the downscaling does not directly affect the climatic fields at low elevation, we also present in Fig. 4 a normalised Taylor diagram computed from the mountainous grid points (elevation greater than 800 m – triangles) only. With this, we see that the downscaling increases the agreement with ERA-interim for mountainous grid points whilst its impact for the whole grid is relatively limited. Interestingly, with and without the downscaling, the performance of the model is better when the lowlands are discarded. This is because the major model biases are located in low land areas (e.g. more than 10 degrees around Hudson Bay). Finally, on the native model grid (outlined-only circles), the downscaling does not impact significantly the model performance.

### 10 3.2.2 Precipitation

The annual mean precipitation rate for CRU CL-v2 and the model is shown in Fig. 5. The model reproduces some of the major large scale structures: East to West decrease in precipitation from the Eastern coast of North America, wet Rocky mountains and relatively wet Western Europe. However, the model presents important biases in some places. In particular, Eastern Siberia, the Southern part of the Rocky mountains and Eastern North America are largely too wet compared to the CRU CL-v2 dataset. The model is conversely too dry in Eastern Europe or central North America. CRU CL-v2 presents a very narrow band (less than 200 km) of extremely high precipitation rate on the Western part of North America. Similarly, a narrow band of high precipitation is observed along the Norwegian coast. These fine scale structures are not captured by the model, in its control version CTRL nor in the downscaling experiments. Where the CTRL simulation fails at reproducing the precipitation maximas over topographic features, the downscaling produces much more spatial variability in better agreement with CRU CL-v2. Generally, the main effect of the downscaling is to increase the precipitation over elevated areas. As such, we are able to mimic the precipitation pattern in Western Europe with precipitation maximas over the Alps, the Scandinavian mountains or the British Highlands. However, the corresponding precipitation maximas in the observations do not necessarily perfectly coincide with the simulated ones: in the observations, the wind-faced coasts present generally more precipitation than the interior grid cells, whilst the downscaling method simulates more precipitation all over elevated grid cells. Over Greenland, the pattern is much better than in the standard version with an increased South to North precipitation decrease. Even if the Northern part of Greenland is still wetter than the observations, it is drier than in the standard version of the model. Over the Rocky mountains, DOWN<sub>020</sub> reproduces some of the local features (Columbia mountains high precipitation), however, the intrinsic model biases are generally not corrected. Where the model tends to be too wet (Eastern Siberia, Alaska or Southern Rocky mountains) the DOWN<sub>ijk</sub> experiments are generally also too wet. This is particularly true where the topography is pronounced (Southern Rocky mountains).

In Fig. 6, we present the annual mean precipitation rate across selected transects. For all the selected transects, but in particular in Europe, the CTRL experiment presents too smooth variations of the precipitation. The different downscaling versions simulate much more variability, coinciding with topography variations. The fit with observations is relatively good in Europe.



This could be explained by the relatively small bias in the CTRL experiment in this region. In North America, the downscaling is improving the precipitation in the Eastern part. In the West, the downscaling tends to increase the wet bias present in the CTRL experiment. For Greenland, the CTRL simulations produce a precipitation maxima at the summit of the ice sheet which corresponds to the precipitation minima in CRU CL-v2. Conversely, the Western flank of the ice sheet for this transect is too dry in the CTRL experiment. The downscaling considerably increases the precipitation at the West margin and produces a meridional precipitation gradient in better agreement with the observations. Also, for specific parameter combinations, we are able to reduce the wet bias in the central part of the ice sheet. However, the model is largely too wet over central Greenland. This might be due to dynamical features not captured by the T21 grid: the coarse resolution facilitates the advection of warm and moist air at the summit of the ice sheet.

10

A quantitative analysis of model performance is shown on Fig. 7 in which we present normalised Taylor diagrams for the CTRL and a selection of  $\text{DOWN}_{ijk}$  experiments against CRU CL-v2. On the NH40 grid (filled circles), most of  $\text{DOWN}_{ijk}$  improves model performance on one specific metric but not necessarily the others. In particular, a lower value for  $\alpha_q^{min}$  tends to reduce the RMSE and to increase the spatial correlation, whilst the standard deviation is reduced. A lower value for  $f_s$  also reduces the RMSE and the standard deviation but has almost no impact on the correlation. The parameter  $z_q$  has a similar effect, but smaller in amplitude, than  $f_s$  in the range tested (not shown). The real addition of the downscaling is the better representation of precipitation for mountainous grid cells (elevation greater than 800 m – filled triangles). In this case, all the downscaling experiments present a better agreement with CRU CL-v2. The spatial correlation is in particular generally greatly improved. On the original model resolution (outlined-only symbols), some selected downscaling experiments present an overall improvement. Generally, the downscaling has a non negligible impact on the precipitation fields on the T21 grid. For multi-millenia integrations, these changes on the hydrological cycle can have important feedbacks on the simulated climate. This means that a new tuning of the model parameters should be performed. In order to avoid this, for further applications the parameters of the  $\text{DOWN}_{020}$  experiment are preferred because they produce an overall improvement of all metrics on the NH40 grid whilst they have a very minor changes from the CTRL experiment on the T21 grid.

25

#### 4 Summary and perspectives

We have presented the inclusion of a dynamical downscaling of heat, temperature and moisture on a 40kmx40km grid of the Northern Hemisphere into a T21 resolution atmospheric model of intermediate complexity. The relevant parts of the model physics needed for the temperature and precipitation are duplicated on the high resolution grid. An upscaling is performed from the high resolution precipitation and temperature, which takes into account the climatic feedback of sub-grid precipitation on the native grid climate. The scheme is conservative and, as such, is suitable for long-term integration.

30



We tested various parameters related to the temperature and precipitation at high resolution. The temperature is only locally impacted by the downscaling with a cooling over mountainous areas. For the precipitation, we have shown that we are able to generate a field at high resolution which presents a better agreement with observations compared to the native coarse resolution atmosphere for mountainous region. The downscaling drastically increases spatial variability compared to the standard version of the model. The model performance is best when the biases in the standard version are low. The downscaling is thus unable to correct for large scale model biases. These biases include biases in atmospheric circulation and model simplification. In particular, the model presents only one moist layer and has no explicit representation of clouds. Further development could include an iterative scheme for clouds and relate clouds to precipitation. Such a development could be tested in the high resolution grid with a specific calibration of convective clouds based on topography. An other model limitation is the lack of diurnal cycle. This can be a reason for the relatively large precipitation data-model mismatch for coastal areas where sea breeze can initiate convection.

From the downscaled atmospheric fields, we are now able to compute the surface mass balance required by the ice sheet model embedded in *i*LOVECLIM. In earlier version of the ice sheet coupled version, Roche et al. (2014) show the poor performance of the surface mass balance computed from bilinearly interpolated precipitation in simulating the present-day Greenland ice sheet topography. The same model validation has now to be done again with the downscaling methodology presented here. However, our methodology is not grid-specific and can be used to compute high resolution temperature and precipitation required for any submodel. Thus, foreseen applications include the computation of high resolution terrestrial water cycle, in particular for permafrost dynamics.

## 20 5 Code availability

The *i*LOVECLIM source code is based on the LOVECLIM model version 1.2 whose code is accessible at <http://www.elic.ucl.ac.be/modx/elic/index.php?id=289>. The developments on the *i*LOVECLIM source code are hosted at <https://forge.ipsl.jussieu.fr/ludus>, but are not publicly available due to copyright restrictions. Access can be granted on demand by request to D. M. Roche ([didier.roche@lsce.ipsl.fr](mailto:didier.roche@lsce.ipsl.fr)) to those who conduct research in collaboration with the *i*LOVECLIM users group. For this work we used the model at revision 706.

*Author contributions.* A. Quiquet, D.M. Roche, C. Dumas and D. Paillard designed the project. A. Quiquet and D.M. Roche implemented the new functionality in *i*LOVECLIM v1.1. A. Quiquet performed the simulations. All authors participated in the analysis of model outputs and the manuscript writing.

*Acknowledgements.* This is a contribution to ERC project ACCLIMATE; the research leading to these results has received funding from the European Research Council under the European Union's Seventh Framework Programme (FP7/2007-2013)/ERC grant agreement 339108.



The authors gratefully thank M. Vrac and K. Izumi for fruitful discussions. We acknowledge the Institut Pierre Simon Laplace for hosting the iLOVECLIM model code under the LUDUS framework project (<https://forge.ipsl.jussieu.fr/ludus>).



## References

- Amante, C. and Eakins, B.: ETOPO1 1 Arc-Minute Global Relief Model: Procedures, Data Sources and Analysis, NOAA Technical Memorandum NESDIS NGDC-24, National Geophysical Data Center, NOAA, 2009.
- Archer, D. and Brovkin, V.: The millennial atmospheric lifetime of anthropogenic CO<sub>2</sub>, *Climatic Change*, 90, 283–297, doi:10.1007/s10584-008-9413-1, 2008.
- 5 Bouttes, N., Roche, D. M., Mariotti, V., and Bopp, L.: Including an ocean carbon cycle model into iLOVECLIM (v1.0), *Geosci. Model Dev.*, 8, 1563–1576, doi:10.5194/gmd-8-1563-2015, 2015.
- Bügelmayer, M., Roche, D. M., and Renssen, H.: Representing icebergs in the iLOVECLIM model (version 1.0) – a sensitivity study, *Geosci. Model Dev.*, 8, 2139–2151, doi:10.5194/gmd-8-2139-2015, 2015.
- 10 Calov, R., Ganopolski, A., Petoukhov, V., Claussen, M., Brovkin, V., and Kubatzki, C.: Transient simulation of the last glacial inception. Part II: sensitivity and feedback analysis, *Climate Dynamics*, 24, 563–576, doi:10.1007/s00382-005-0008-5, 2005.
- Charbit, S., Kageyama, M., Roche, D., Ritz, C., and Ramstein, G.: Investigating the mechanisms leading to the deglaciation of past continental northern hemisphere ice sheets with the CLIMBER GREMLINS coupled model, *Global and Planetary Change*, 48, 253–273, 2005.
- Claussen, M., Mysak, L. A., Weaver, A. J., Crucifix, M., Fichet, T., Loutre, M.-F., Weber, S. L., Alcamo, J., Alexeev, V. A., Berger, A., Calov, R., Ganopolski, A., Goosse, H., Lohmann, G., Lunkeit, F., Mokhov, I. I., Petoukhov, V., Stone, P., and Wang, Z.: Earth system models of intermediate complexity: closing the gap in the spectrum of climate system models, *Climate Dynamics*, 18, 579–586, 2002.
- 15 Dee, D. P., Uppala, S. M., Simmons, A. J., Berrisford, P., Poli, P., Kobayashi, S., Andrae, U., Balmaseda, M. A., Balsamo, G., Bauer, P., Bechtold, P., Beljaars, A. C. M., van de Berg, L., Bidlot, J., Bormann, N., Delsol, C., Dragani, R., Fuentes, M., Geer, A. J., Haimberger, L., Healy, S. B., Hersbach, H., Hólm, E. V., Isaksen, L., Kållberg, P., Köhler, M., Matricardi, M., McNally, A. P., Monge-Sanz, B. M., Morcrette, J.-J., Park, B.-K., Peubey, C., de Rosnay, P., Tavolato, C., Thépaut, J.-N., and Vitart, F.: The ERA-Interim reanalysis: configuration and performance of the data assimilation system, *Quarterly Journal of the Royal Meteorological Society*, 137, 553–597, doi:10.1002/qj.828, 2011.
- 20 Ettema, J., Broeke, M. R. v. d., Meijgaard, E. v., Berg, W. J. v. d., Bamber, J. L., Box, J. E., and Bales, R. C.: Higher surface mass balance of the Greenland ice sheet revealed by high-resolution climate modeling, *Geophysical Research Letters*, 36, 5 PP., doi:200910.1029/2009GL038110, 2009.
- Fyke, J. G., Weaver, A. J., Pollard, D., Eby, M., Carter, L., and Mackintosh, A.: A new coupled ice sheet/climate model: description and sensitivity to model physics under Eemian, Last Glacial Maximum, late Holocene and modern climate conditions, *Geoscientific Model Development*, 4, 117–136, 2011.
- Goelzer, H., Huybrechts, P., Loutre, M.-F., and Fichet, T.: Last Interglacial climate and sea-level evolution from a coupled ice sheet-climate model, *Clim. Past*, 12, 2195–2213, doi:10.5194/cp-12-2195-2016, 2016.
- 30 Goosse, H., Brovkin, V., Fichet, T., Haarsma, R., Huybrechts, P., Jongma, J., Mouchet, A., Selten, F., Barriat, P.-Y., Campin, J.-M., Deleersnijder, E., Driesschaert, E., Goelzer, H., Janssens, I., Loutre, M.-F., Morales Maqueda, M. A., Opsteegh, T., Mathieu, P.-P., Munhoven, G., Pettersson, E. J., Renssen, H., Roche, D. M., Schaeffer, M., Tartinville, B., Timmermann, A., and Weber, S. L.: Description of the Earth system model of intermediate complexity LOVECLIM version 1.2, *Geosci. Model Dev.*, 3, 603–633, doi:10.5194/gmd-3-603-2010, <http://www.geosci-model-dev.net/3/603/2010/>, 2010.
- 35 Gregory, J. M., Browne, O. J. H., Payne, A. J., Ridley, J. K., and Rutt, I. C.: Modelling large-scale ice-sheet–climate interactions following glacial inception, *Clim. Past*, 8, 1565–1580, doi:10.5194/cp-8-1565-2012, 2012.



- Haarsma, R. J., Selten, F. M., Opsteegh, J. D., Lenterink, G., and Liu, Q.: ECBILT: A coupled atmosphere ocean sea-ice model for climate predictability studies, KNMI technical report TR-195, De Bilt, The Netherlands, 1997.
- Kitover, D. C., van Balen, R., Roche, D. M., Vandenberghe, J., and Renssen, H.: Advancement toward coupling of the VAMPER permafrost model within the Earth system model iLOVECLIM (version 1.0): description and validation, *Geosci. Model Dev.*, 8, 1445–1460, doi:10.5194/gmd-8-1445-2015, 2015.
- 5 Levavasseur, G., Vrac, M., Roche, D. M., Paillard, D., Martin, A., and Vandenberghe, J.: Present and LGM permafrost from climate simulations: contribution of statistical downscaling, *Climate of the Past*, 7, 1225–1246, doi:10.5194/cp-7-1225-2011, 2011.
- Loutre, M. F., Mouchet, A., Fichet, T., Goosse, H., Goelzer, H., and Huybrechts, P.: Evaluating climate model performance with various parameter sets using observations over the recent past, *Clim. Past*, 7, 511–526, doi:10.5194/cp-7-511-2011, 2011.
- 10 Luthi, D., Le Floch, M., Bereiter, B., Blunier, T., Barnola, J.-M., Siegenthaler, U., Raynaud, D., Jouzel, J., Fischer, H., Kawamura, K., and Stocker, T. F.: High-resolution carbon dioxide concentration record 650,000–800,000 years before present, *Nature*, 453, 379–382, doi:10.1038/nature06949, 2008.
- New, M., Lister, D., Hulme, M., and Makin, I.: A high-resolution data set of surface climate over global land areas, *Climate Research*, 21, 1–25, doi:10.3354/cr021001, 2002.
- 15 Opsteegh, J. D., Haarsma, R. J., Selten, F. M., and Kattenberg, A.: ECBILT: a dynamic alternative to mixed boundary conditions in ocean models, *Tellus A*, 50, 348–367, doi:10.1034/j.1600-0870.1998.t01-1-00007.x, 1998.
- Robinson, A., Calov, R., and Ganopolski, A.: An efficient regional energy-moisture balance model for simulation of the Greenland Ice Sheet response to climate change, *The Cryosphere*, 4, 129–144, doi:10.5194/tc-4-129-2010, 2010.
- Roche, D. M.:  $\delta^{18}\text{O}$  water isotope in the iLOVECLIM model (version 1.0) – Part 1: Implementation and verification, *Geosci. Model Dev.*, 20 6, 1481–1491, doi:10.5194/gmd-6-1481-2013, 2013.
- Roche, D. M. and Caley, T.:  $\delta^{18}\text{O}$  water isotope in the iLOVECLIM model (version 1.0) – Part 2: Evaluation of model results against observed  $\delta^{18}\text{O}$  in water samples, *Geosci. Model Dev.*, 6, 1493–1504, doi:10.5194/gmd-6-1493-2013, 2013.
- Roche, D. M., Dumas, C., Bügelmayer, M., Charbit, S., and Ritz, C.: Adding a dynamical cryosphere to iLOVECLIM (version 1.0): coupling with the GRISLI ice-sheet model, *Geosci. Model Dev.*, 7, 1377–1394, doi:10.5194/gmd-7-1377-2014, 2014.
- 25 Schoof, C.: Ice sheet grounding line dynamics: Steady states, stability, and hysteresis, *Journal of Geophysical Research (Earth Surface)*, 112, <http://adsabs.harvard.edu/abs/2007JGRF..11203S28S>, 2007.
- Vetter, T., Huang, S., Aich, V., Yang, T., Wang, X., Krysanova, V., and Hattermann, F.: Multi-model climate impact assessment and inter-comparison for three large-scale river basins on three continents, *Earth System Dynamics*, 6, 17–43, doi:10.5194/esd-6-17-2015, 2015.
- Vizcaíno, M., Mikolajewicz, U., Gröger, M., Maier-Reimer, E., Schurgers, G., and Winguth, A. M. E.: Long-term ice sheet–climate interactions under anthropogenic greenhouse forcing simulated with a complex Earth System Model, *Climate Dynamics*, 31, 665–690, doi:10.1007/s00382-008-0369-7, 2008.
- 30 Vizcaíno, M., Mikolajewicz, U., Jungclaus, J., and Schurgers, G.: Climate modification by future ice sheet changes and consequences for ice sheet mass balance, *Climate Dynamics*, 34, 301–324, doi:10.1007/s00382-009-0591-y, 2010.
- Vrac, M., Marbaix, P., Paillard, D., and Naveau, P.: Non-linear statistical downscaling of present and LGM precipitation and temperatures over Europe, *Clim. Past*, 3, 669–682, doi:10.5194/cp-3-669-2007, 2007.
- Wolff, E. W.: Greenhouse gases in the Earth system: a palaeoclimate perspective, *Philosophical Transactions of the Royal Society of London A: Mathematical, Physical and Engineering Sciences*, 369, 2133–2147, doi:10.1098/rsta.2010.0225, 2011.

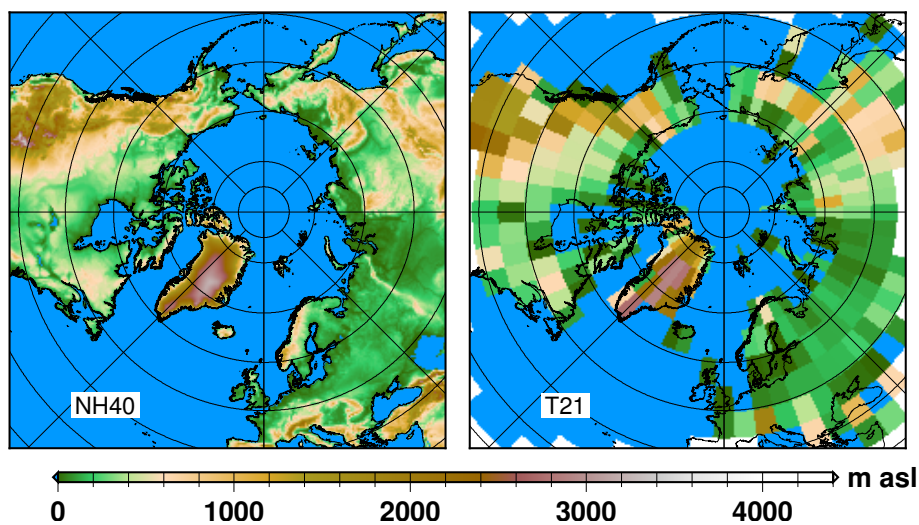


**Figure 1.** Northern Hemisphere topography from ETOPO1 projected with a Lambert equal area on a Cartesian 40kmx40km grid (left) and in the native ECBilt grid (right).

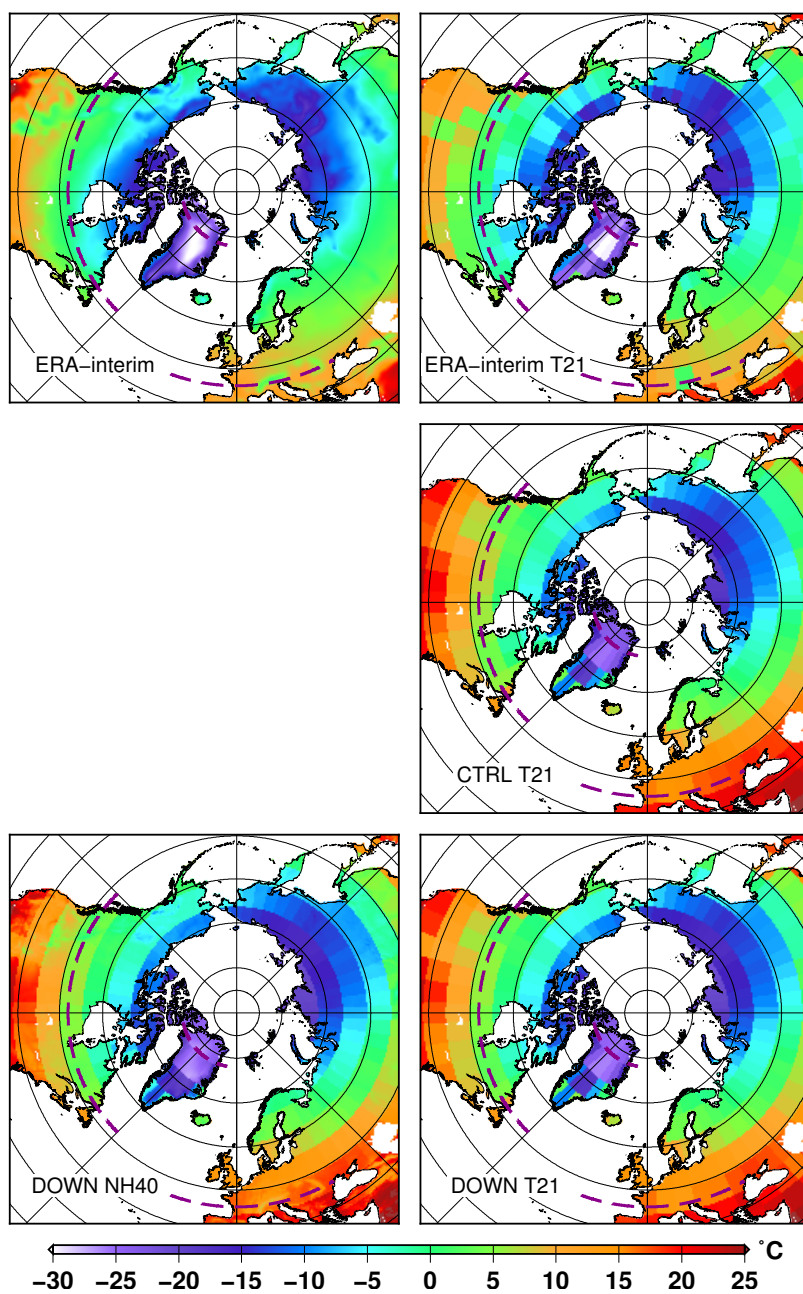


**Figure 2.** Northern Hemisphere annual mean surface temperature (°C) in: ERA-interim (top), the standard version of *i*LOVECLIM (middle, CTRL) and the *i*LOVECLIM that includes a downscaling (bottom, DOWN<sub>020</sub>, with  $z_q = 2000m$ ,  $\alpha_q^{min} = 0.8$  and  $f_s = 0.6$ ). The left panel corresponds to data on the high resolution grid, whilst on the right the data are aggregated to the T21 resolution. The dashed purple lines stand for the selected transects used for discussion.

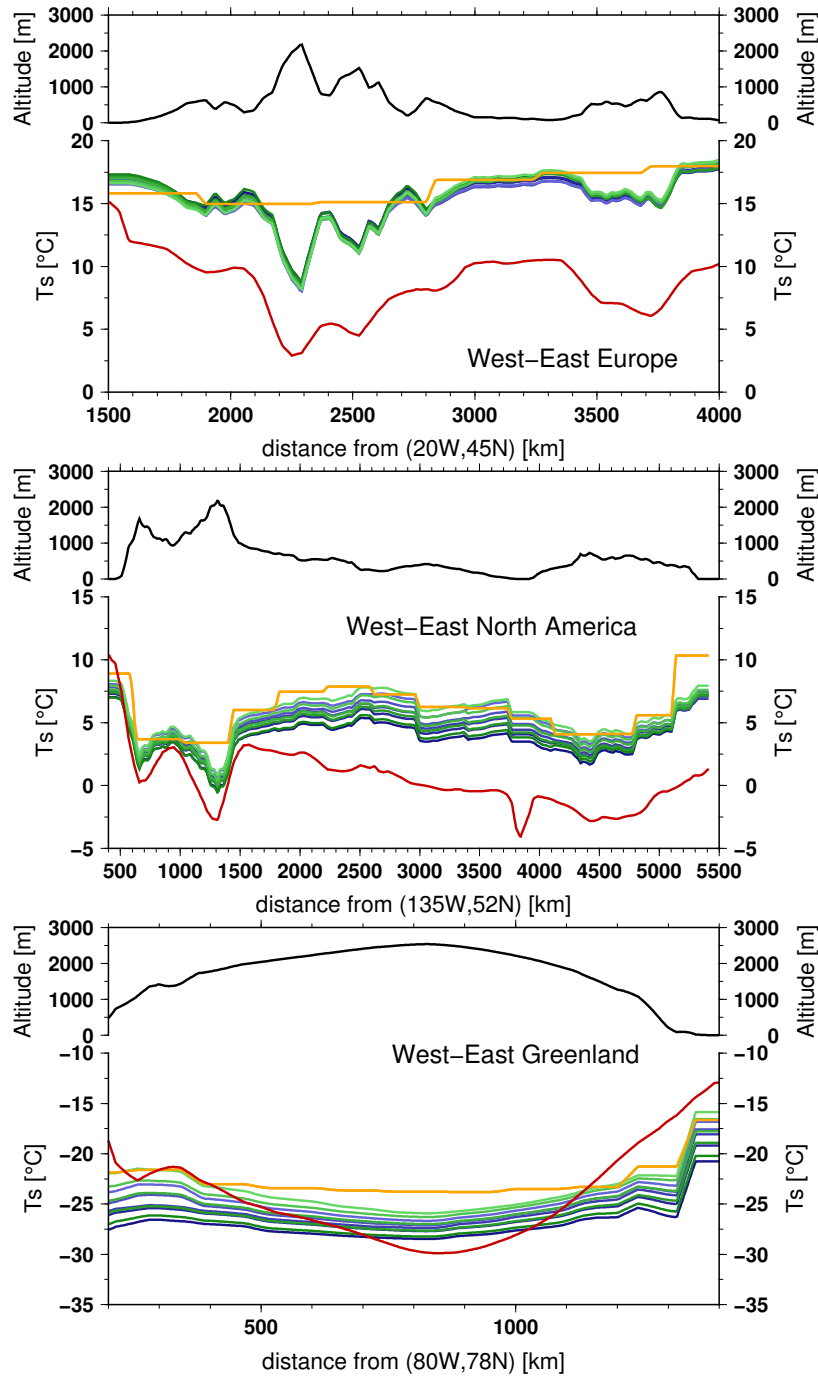


**Figure 3.** Transects for selected regions: Europe (top panel), America (middle panel) and Greenland (bottom panel). The upper part of each panel shows the elevation along the transects. The lower part of each panel depicts the annual mean surface temperature along the transects for: ERA-interim (red), the standard *iLOVECLIM* (CTRL, orange), the *iLOVECLIM* including a downscaling with  $f_s = 1.0$  (blue), the *iLOVECLIM* including a downscaling with  $f_s = 0.6$  (green). The different shades of blue and green correspond to  $\alpha_q^{min}$  ranging from 0.7 (dark) to 0.9 (light). The downscaling experiments presented in this figure use  $z_q = 2000m$  and a change to  $z_q = 3500m$  has only a very limited effect.

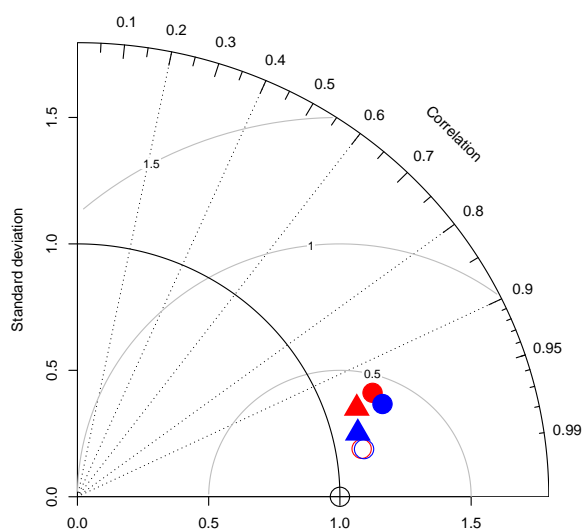


**Figure 4.** Normalised Taylor diagrams on the ERA-interim annual mean surface temperature for the standard CTRL experiment (red) and a selected downscaling experiment ( $DOWN_{020}$ ) (blue). The circles depict the score when all grid points are considered, whilst the triangles stand for points with an elevation greater than 800 m. The filled symbols correspond to the Taylor Diagram computed on the high resolution grid whilst the symbols outlined-only are for the T21 grid.

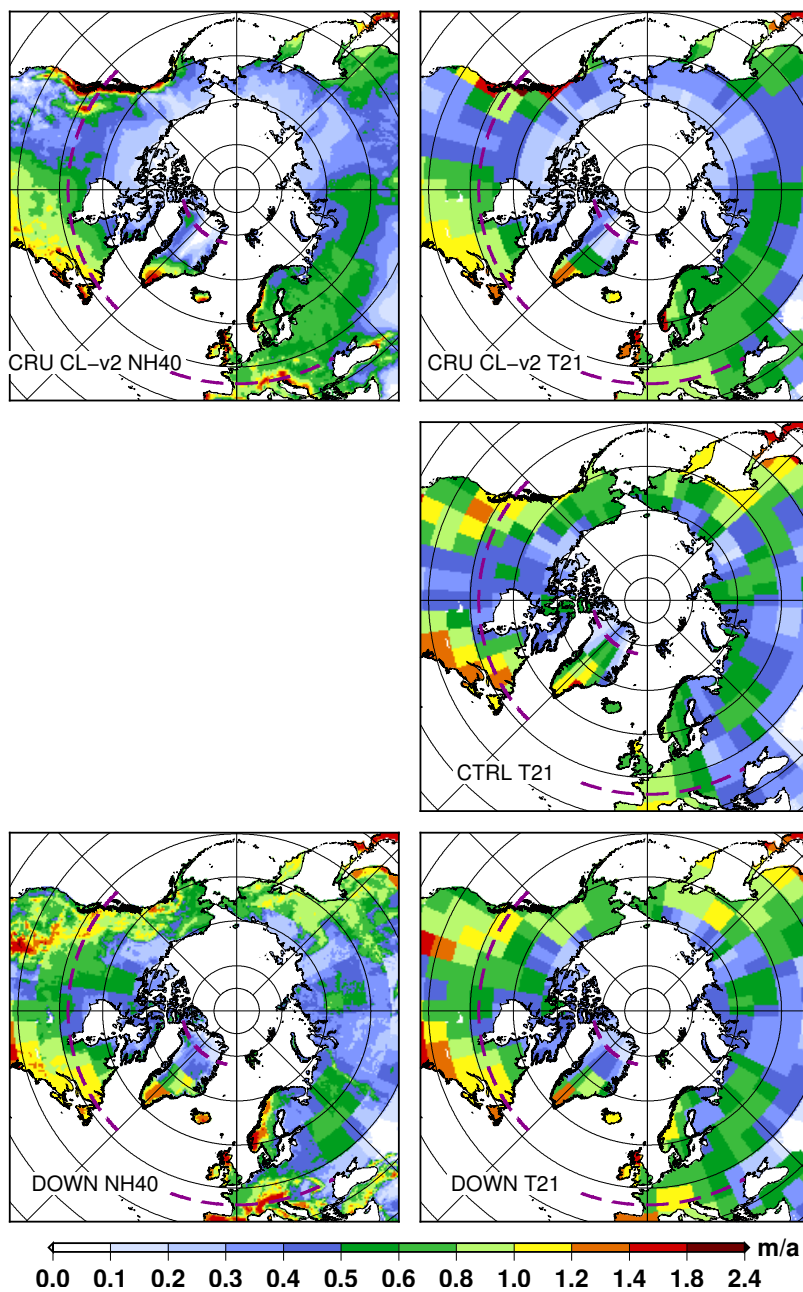


**Figure 5.** Northern Hemisphere annual mean precipitation rate (m/a) in: CRU CL-v2 (top), the standard version of *i*LOVECLIM (middle, CTRL) and the *i*LOVECLIM that includes a downscaling (bottom, DOWN<sub>020</sub>, with  $z_q = 2000m$ ,  $\alpha_q^{min} = 0.8$  and  $f_s = 0.6$ ). The left panel corresponds to data on the high resolution grid, whilst on the right the data are aggregated to the T21 resolution. The dashed purple lines stand for the selected transects used for discussion.

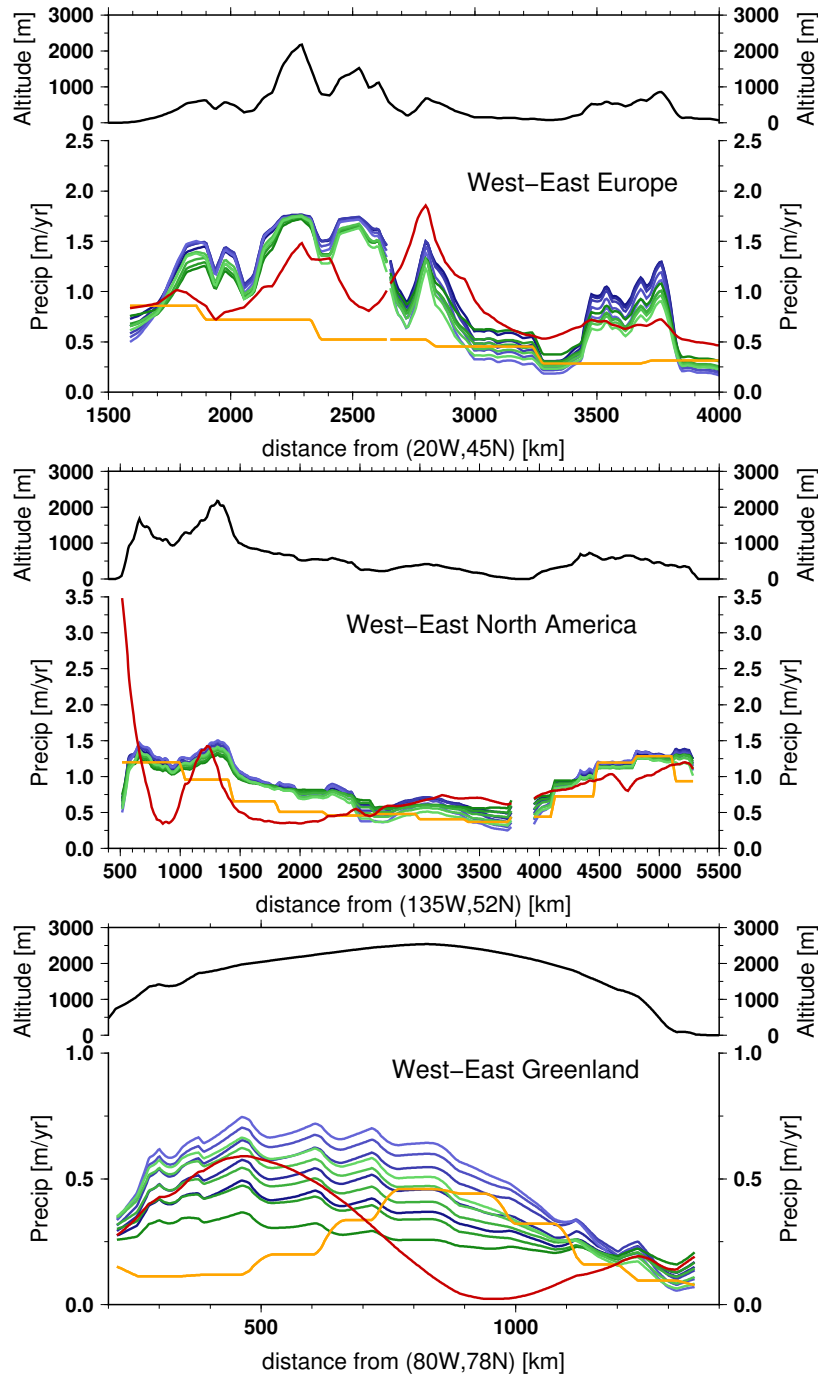


**Figure 6.** Transects for selected regions: Europe (top panel), America (middle panel) and Greenland (bottom panel). The upper part of each panel shows the elevation along the transects. The lower part of each panel depicts the annual mean precipitation along the transects for: CRU CL-V2 (red), the standard *i*LOVECLIM (CTRL, orange), the *i*LOVECLIM including a downscaling with  $f_s = 1.0$  (blue), the *i*LOVECLIM including a downscaling with  $f_s = 0.6$  (green). The different shades of blue and green correspond to  $\alpha_q^{min}$  ranging from 0.7 (dark) to 0.9 (light). The downscaling experiments presented in this figure use  $z_q = 2000m$  and a change to  $z_q = 3500m$  has only a very limited effect.

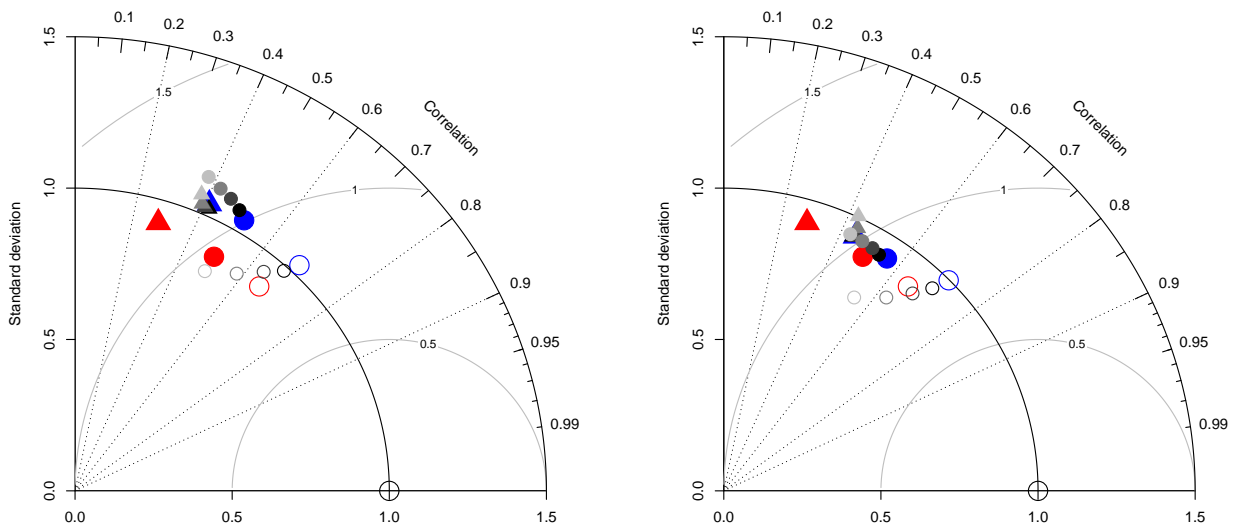


**Figure 7.** Normalised Taylor diagrams on the CRU CL-V2 annual mean precipitation rate for the standard CTRL experiment (red) and a series of  $DOWN_{ijk}$  experiments (grey and blue). The circles depict the score when all grid points are considered, whilst the triangles stand for points with an elevation greater than 800 m. The filled symbols correspond to the Taylor Diagram computed on the high resolution grid whilst the symbols outlined-only are for the T21 grid. All the  $DOWN_{ijk}$  experiments presented here use  $z_q = 2000m$ . The different shades of greys are for different  $\alpha_q^{min}$  ranging from 0.75 (dark) to 0.9 (light), for  $f_s = 1.0$  (left) and  $f_s = 0.6$  (right).  $DOWN_{004}$  (left) and  $DOWN_{000}$  (right) are in blue.